Backstepping-based robust-adaptive control of a nonlinear 2-DOF piezoactuator

Juan-Antonio ESCARENO[1], Micky RAKOTONDRABE[2*], and Didace HABINEZA[2]

[1]: *Polytechnic Institute of Advanced Sciences, 7-9 rue M. Grandcoing, 94200 Ivry-sur-Seine, France.*

[2]: *Automatic Control and Micro-Mechatronic Systems depart. (AS2M), FEMTO-ST Institute, CNRS - University of Franche-Comté at Besançon (UFC) - ENSMM - UTBM, Besançon France.*

[*]: *corresponding author, email: mrakoton@femto-st.fr*

Abstract

This paper deals with the control of a two degrees of freedom (2-DOF) piezoelectric actuator for precise positioning and which exhibits strong hysteresis nonlinearity and strong cross-couplings. To tackle the nonlinearity and the cross-couplings, we propose two decoupled models in which they are considered as (fictive) external disturbances which require proper characterization. Then, a backstepping technique is proposed to construct a robust controller that merges sliding-mode and adaptive schemes. Extensive experimental tests are finally carried out to prove the efficiency of the modeling and control technique proposed.

Key words: Piezoelectric actuator, 2 degrees of freedom, hysteresis nonlinearity, cross-couplings, backstepping technique, merged sliding mode and adaptive schemes, robust controller.

1 INTRODUCTION

The significant advance of fabrication and manipulation of micro/nano objects in recent years, from technological and theoretical point of view, has increased the application range in many fields (biology, medicine, automotive, aeronautics and aerospace, data-storage, etc). One of the main challenge when working at micro/nano scale is the ability to execute tasks with a relatively high operating speed and a very high positioning precision. Piezoelectric based actuators are the most useful tools for such applications, mainly due to the high resolution, the wide operating bandwidth and the significant stiffness

they can offer. The most known application of piezoelectric actuators is the surface scanning at atomic scale with scanning tunneling microscope [1] and atomic force microscope [2]. In these two applications, a piezoelectric tube scanner [3] is used in order to make possible the exploration of the scanned sample with a nanometric resolution. Alternatively, this task can also be ensured by compliant structures [4,5] driven by piezoelectric stack actuators [6]. Another well-known category of piezoelectric actuators includes microgrippers [7,8] which are generally made of two cantilevered piezoelectric actuators, allowing them to be used for manipulation or handling of micro-objects. They are very used for the execution of pick-and-place tasks in the field of micromanipulation and microassembly [9]. From the aforementioned categories and applications of piezoelectric actuators, it is worth to mention that some of them are designed to provide deflections (displacements) along one direction/axis, i.e. one degree of freedom (1-DOF or monovariable) piezoelectric actuators. Examples include unimorph piezoelectric cantilevers and piezoelectric stacks. Other actuators are designed to handle surface or spatial tasks by providing displacements along different directions: multi-DOF (multivariable) piezoelectric actuators. Examples include duo-bimorph and duo-multimorph piezoelectric cantilevers, piezoelectric tubes scanners.

Despite the advantages, variety and the wide range of applications cited above, piezoelectric based actuators typify adverse nonlinear effects (hysteresis and creep) making the control design often a complex task [10, 11]. In addition, strong couplings appear between the different axes in multi-DOF piezoelectric actuators, resulting in an additional cause of positioning inaccuracy. The problem here is that these nonlinearities, i.e. the hysteresis and the creep, which are present in the expected actuator displacements (or direct transfers), also appear in these couplings [10, 12–14]. It is worth also highlighting that systems, in practice, feature amplitude-limited inputs [15, 16]. This aspect must be considered in the control design for stability purposes. For these reasons, it is necessary to develop appropriate control designs that not only take into account inherent nonlinearities and couplings between the piezoelectric actuators axis but also the bounded control inputs.

Dealing with piezoelectric systems featuring hysteresis and creep nonlinearities has been addressed using feedback and feedforward control strategies, or, the combination of both. Feedforward control relies on precise models and their inverses or approximate inverses as compensator of the hysteresis or of the creep. In feedback, the litterature is abundant and techniques from classical schemes to more advanced like robust/adaptive schemes which regard or disregard the hysteresis or creep models have been used. The main advantages of feedback techniques are indeed the robustness and the disturbances rejection they can offer.

In feedback control schemes, techniques mainly included PID [17–19], lin-

ear robust control methods [20–25] and other control techniques such as, Lyapunov-based Sliding Mode Control (SMC), iterative, adaptive and repetitive control schemes [26–35]. However, when there is a lack of conventient sensors to perform the feedback, for instance for certain miniaturized positioning systems for which there are no embeddable sensors with the required performances, feedforward control scheme is often used instead of feedback.

In feedforward control, the most used models of hysteresis and the related compensators are based on the superposition of elementary hysteresis called hysterons. They are the Preisach [36–39] and the Prandtl-Ishlinskii approaches [40–45]. The open-loop compensator, i.e. the hysteresis inverse model, is afterwards computed using the identified model. The two approaches can be very accurate subject to the use of a high number of hysterons. Another family of hysteresis models is based on differential equations. The sole utilized in modeling and compensation is the Bouc-Wen model [46, 47] which has an advantage of simplicity and ease of identification. The synthesis of the open-loop compensator in Bouc-Wen approach has been carried out in [14, 48].

The creep nonlinearity has been modeled as a series of spring-damper systems resulting in a linear dynamic model [49]. This linear dynamic model can be directly inverted when it satisfies the bi-causality and bi-stability properties in order to compensate for the creep [50, 51]. The inverse multiplicative structure has also been used in [13, 43] allowing the use of the identified dynamic model itself as compensation, i.e. without extra-calculation of the inverse model. In [52, 53], the logarithmic model has been used to model and to compensate for the creep. Nevertheless, open-loop controlled systems are not robust and can not handle the models uncertainties as well as external disturbances. Therefore, feedforward techniques can not be employed in certain applications where the models utilized may vary during the functioning, where the identified models are not precise enough or where external disturbances are present. This is why feedforward schemes are increased with feedback schemes in these applications to increase the robustness and to reach some specified performances that could not be attained with feedback or feedforward individually [10, 12, 54–59].

The contribution of this paper is the modeling and the proposition of an alternative control strategy for a 2-DOF piezoelectric cantilevered actuator to perform complex trajectories and waypoint trackings evolving in the planar space (y and z axes). The 2-DOF piezoactuator is mainly utilized in precise positioning such as micromanipulation and microassembly. The tasks consist principally to manipulate, to pick-transport-and-place or to assemble artificial (non-biological) objects of sizes ranging between tens of microns to a few of millimeters. These tasks require very high resolution of positioning, an accuracy better than the micron, a manipulation force generally ranging between 100μN and 40mN and a bandwidth in excess of a ten of Hertz

[9]. Based on PZT (lead-zirconate-titanate) piezoelectric material, the 2-DOF piezoactuator was a good candidate for these tasks since it can perform up to 30mN of force, nanometric resolution, and a bandwidth of hundreds of Hertz. additionally to that, the two degrees of freedom of the actuator permits to perform dexterous micromanipulation. As adverse side however, the 2-DOF piezoactuator exhibits a strong nonlinear phenomenon (hysteresis) and strong cross-couplings between the two axes. In fact, it is observed that the cross-couplings dramatically distort the motion of the actuator. These phenomena strongly compromise the accuracy, and even the stability of the final tasks to be performed. We propose in this paper a modeling and control technique that permits to account for the hysteresis and for these strong-couplings to make the 2-DOF piezoactuator reach the performances required in precise positioning like micromanipulation or microassembly tasks. More precisely, we propose to rassemble the hysteresis and the cross-couplings in a single parameter considered as external disturbances and that will be taken into account during the controller design. For that, the Backstepping technique is used to merge sliding-mode and adaptive control schemes to overcome the adverse effects of the disturbances associated to the actuator's biaxial displacement. The principal advantage of the proposed modeling technique and control strategy is that there is no requirement to have a specific knowledge on the nonlinearities. Only norms that bound them are required during the proposed controller synthesis. Similarly, there is no requirement of a precise knowledge on the cross-couplings, contrary to the models in feedforward and in feedforward-feedback combined techniques. All this renders the proposed modeling among the most simple techniques but robust in the control law. Different and extensive experiments are carried out to demonstrate the efficiency of the method, in particular at different frequencies. Discussions with regards to the proposed controller gains calculation, to the experimental results and to the comparison of the method with classical controller design are presented.

The remainder of the paper is organized as follows. The modeling of the piezoelectric cantilevered actuator (piezoactuator) is presented in section-2. We particularly show in this section the derivation of the model with lumped parameter that rassembles the hysteresis nonlinearity and the cross-couplings. In section-3 the description of the experimental setup is provided. Section-4 presents the robust-adaptive control to counteract the disturbances accomplishing the control objective. Experimental results and discussions are presented in section-5. Lastly, the conclusions and perspectives are given in section-6.

2 Modeling of a 2-DOF piezoactuator

A piezoelectric cantilevered actuator (piezoactuator) is a cantilever with rectangular section and which has one or several layers. The layers can be piezoelectric (active layer or piezolayer) or non-piezoelectric (passive layer). Whilst the lead-zirconate-titanate (PZT) ceramics is often used as piezolayers, chromium, copper and silicone are used as passive ones. The bending of the piezoactuator, which is the output displacement, is obtained as a result of the difference between the longitudinal strains of the different layers (passive and piezolayers) due to the application of an electric voltage. Fig. 1-a presents the case of a 1-DOF actuator with two layers: one passive layer and one active layer. In this, the application of a voltage U to the piezolayer yields its contraction/expansion. Due to the interface constraint between the two layers, a bending δ is finally obtained. As described in the introduction, the dynamic modeling including the hysteresis nonlinearity has been widely studied. Schematically, as represented in Fig. 1-b, such dynamic model is composed of a static nonlinearity $H(U(s))$ (or simply $H(U)$) that tracks the hysteresis in piezoelectricity and a linear dynamics $D(s)$ (s being the Laplace variable) of the whole plant. This scheme is called Hammerstein approximation and is widely admitted in the litterature. In the figure, δ_s is the static output displacement without consideration of the plant dynamics. In the next subsections, we will model the hysteresis $H(U)$ and the dynamics $D(s)$. Then we will extend the model in order to introduce the cross-couplings in 2-DOF actuators. The model is afterwards used to derive a model where the nonlinearities and the cross-couplings are rassembled in a bounded disturbance parameter. This latter model will finally be used in section-3 for the controller synthesis.

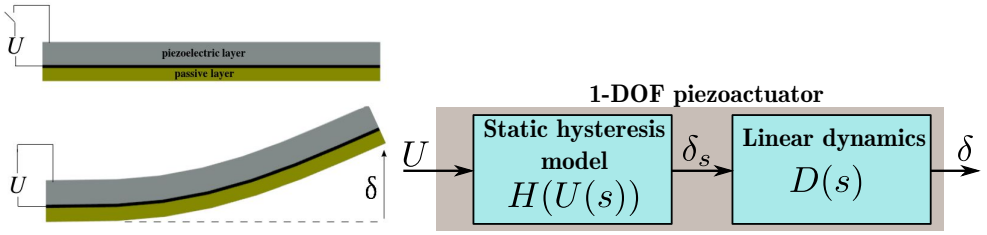

(a) (b)

Fig. 1. (a): deflection δ of a 1-DOF cantilevered piezoactuator due to an external input U. (b): Hammerstein block-scheme of the 1-DOF piezoactuator.

2.1 Nonlinear Bouc-Wen model of the hysteresis in 1-DOF piezoactuators

Numerous models are available to describe the hysteresis $H(U)$ of piezoactuators The Bouc-Wen model of hysteresis not only provides an interesting simplicity in terms of computation and implementation, but also, can represent a wide hysteresis classes. In addition, the Bouc-Wen model is particularly well suited for structural analysis (stability, performances) and controllers synthesis [14, 48].

First, the static nonlinearity $\delta_s = H(U)$ is described. The Bouc-Wen static model of hysteresis adapted to piezoactuators is described by [48, 60]:

$$\begin{cases} \delta_s(t) = d_p U(t) - h(t) \\ \dot{h}(t) = d_p A_{bw} \dot{U}(t) - B_{bw} \left|\dot{U}(t)\right| h(t) - C_{bw} \dot{U}(t) \left|h(t)\right| \end{cases} \tag{1}$$

where A_{bw}, B_{bw} and C_{bw} are coefficients determining the hysteresis shape and amplitude and d_p is a positive coefficient that defines the magnitude deflection. The signal $h(t)$ represents the hysteresis internal state. The first equation is the output equation whilst the second equation (nonlinear and differential) is the state equation of the hysteresis.

On the other hand, the transient dynamic part of a piezoactuator can be approximated by a second-order system, that is:

$$a\ddot{\delta}(t) + b\dot{\delta}(t) + \delta(t) = \delta_s(t) \tag{2}$$

where a and b are coefficients obtained from an identification procedure. The dynamics is easily derived: $D(s) = \frac{1}{as^2+bs+1}$.

The final nonlinear dynamic model is therefore:

$$\begin{cases} a\ddot{\delta} + b\dot{\delta} + \delta = d_p U - h \\ \dot{h} = d_p A_{bw} \dot{U} - B_{bw} \left|\dot{U}\right| h - C_{bw} \dot{U} \left|h\right| \end{cases} \tag{3}$$

2.2 Extension of the model for 2-DOF piezoactuators

The previous model is valuable for 1-DOF piezoactuators. The aim of this paper being the modeling and control of a 2-DOF piezoactuator devoted to precise positioning, we propose to extend the previous model. Consider Fig. 2

which represents the block-diagram of a 2-DOF piezoactuator with the input vector $U = \begin{pmatrix} U_y & U_z \end{pmatrix}^T$ and the output vector $\delta = \begin{pmatrix} \delta_y & \delta_z \end{pmatrix}^T$. The axes of displacement (bending) of the piezoactuator are y and z. If we consider that there are no cross-couplings between the two axes, the displacement model along each axis is directly yielded from (3):

$$\begin{cases} a_i\ddot{\delta}_i + b_i\dot{\delta}_i + \delta_i = d_{pi}U_i - h_i \\ \dot{h}_i = d_{pi}A_{bwi}\dot{U}_i - B_{bwi}\left|\dot{U}_i\right| h_i - C_{bwi}\dot{U}_i\left|h_i\right| \end{cases} \tag{4}$$

where $i \in \{y, z\}$.

However, as we will see in the experimental characterizations in the next sections, there are cross-couplings between axes y and z that make the model (4) not applicable. In addition, these cross-couplings are also nonlinear. Let us denote $\mathcal{C}_i(U_j, h_j)$, with $i \in \{y, z\}$ and $j \in \{y, z\} - i$, the coupling found in the axis i and which is due to the voltage U_j. Thus, the displacement model along each axis is taken from (4) in which we add the cross-coupling expression:

$$\begin{cases} a_i\ddot{\delta}_i + b_i\dot{\delta}_i + \delta_i = d_{pi}U_i - h_i + \mathcal{C}_i(U_j, h_j) \\ \dot{h}_i = d_{pi}A_{bwi}\dot{U}_i - B_{bwi}\left|\dot{U}_i\right| h_i - C_{bwi}\dot{U}_i\left|h_i\right| \end{cases} \tag{5}$$

which is rewritable as:

$$a_i\ddot{\delta}_i + b_i\dot{\delta}_i + \delta_i = d_{pi}U_i + \Theta_i \tag{6}$$

where $\Theta_i = -h_i + \mathcal{C}_i(U_j, h_j)$ will be assumed as bounded and varying signal in the sequel. It is worth to notice that the creep nonlinearity is additive relative to the hysteresis [20, 43]. Thus, it can also be rassembled in Θ_i, i.e. $\Theta_i = -h_i + \mathcal{C}_i(U_j, h_j) + C_{cri}(U_i) + C_{cri}(U_j)$ where $C_{cri}(U_i)$ is the creep in the direct transfer and $C_{cri}(U_j)$ is the coupling creep. Since the creep in piezoelectric actuators is bounded [61], we have Θ_i still bounded.

In a matrix form, (6) is equivalent to:

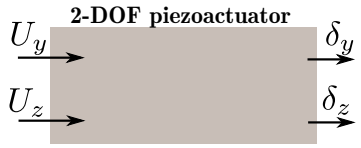

Fig. 2. A 2-DOF piezoactuator.

$$a\ddot{\delta} + b\dot{\delta} + \delta = d_p U + \Theta \tag{7}$$

where $a = diag\,(a_y, a_z)$, $b = diag\,(b_y, b_z)$ and $d_p = diag\,(d_{py}, d_{pz})$. We have: $\delta = (\delta_y, \delta_z)^T$, $U = (U_y, U_z)^T$ and $\Theta = (\Theta_y, \Theta_z)^T$.

Notice that in the matrix form, the state equation of the hysteresis and which is a part of Θ is [1] :

$$\dot{h} = d_p A_{bw} \dot{U}(t) - B_{bw} \left(\left| \dot{U}(t) \right| \circ h(t) \right) - C_{bw} \left(\dot{U}(t) \circ |h(t)| \right) \tag{8}$$

where $h = (h_y, h_z)^T$, $A_{bw} = diag\,(A_{bwy}, A_{bwz})$, $B_{bw} = diag\,(B_{bwy}, B_{bwz})$ and $C_{bw} = diag\,(C_{bwy}, C_{bwz})$.

As we can see from the model in (7), the cross-couplings and the nonlinearities (hysteresis and eventual creep) can be rassembled in a bounded parameter Θ. The model (7) will be employed in the next section-4 to calculate a control law where Θ is considered as bounded disturbance. As the bound of the parameter Θ is taken into account during the control design, the yielded controller will be robust face to the hysteresis and creep nonlinearities and to the cross-couplings between the axes.

3 Experimental setup and characterization

3.1 Experimental setup

The experimental setup is based on a piezoelectric cantilevered actuator able to bend along the y axis and along the z axis, see Fig. 3-a. This piezoactuator has a rectangular section and its total dimensions are: 27mm ×1mm ×0.91mm. The active length (length out off the clamping) is 25mm which permits to obtain a relatively large displacement with only ±10V of voltage inputs. Two inductive sensors from *IBS*-company are utilized to measure the bendings of the actuator. The sensors are tuned to have a resolution of about 100nm and a bandwidth of 1.5kHz which are sufficient enough for the experiments carried out in this paper. Each sensor as well as the actuator are supported by a proper x-y-z manual and precise stage that permits to adjust their relative position. We employ a computer and dSPACE board acquisition system to manage the different signals and to implement the controllers through the

[1] $(X \circ Y)$ denotes the Hadamard product of vectors $X = [X_{ij}]_{i,j}$ and $Y = [Y_{ij}]_{i,j}$, *i.e.*$(X \circ Y) = [X_{ij} Y_{ij}]_{i,j}$

Matlab-Simulink software. The sampling period is set equal to 0.2ms which is sufficiently low to account for the dynamics of the actuator. Since the input voltages do not exceed ±10V, no amplifier is required. Fig. 3-b depicts the diagram of the setup.

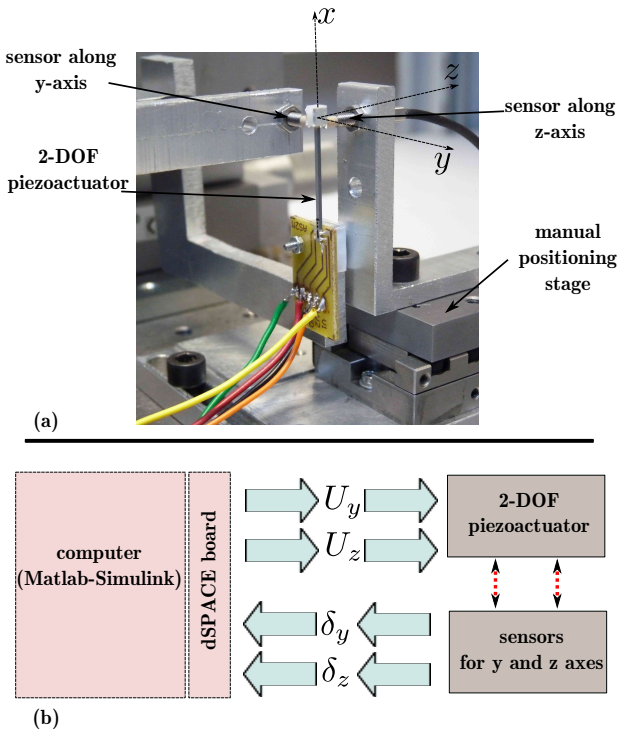

Fig. 3. (a): the 2-DOF piezoactuator. (b): diagram of the experimental setup.

3.2 Characterization

First, the behavior of the piezoactuator is characterized. The aim is to evaluate the cross-couplings between the axes and the hysteresis nonlinearities in them. For that, a sine input voltage $U_y(t) = 10\sin(2\pi ft)$ is applied to the y axis first, with U_z left equal to zero. The frequency is chosen to be $f = 1$Hz, which is convenient to start the hysteresis characterization. Then, the resulting displacement δ_y is reported and the direct transfer in the (U_y, δ_y)-map can be plotted (see Fig. 4-a with solid-circle plot). In the meantime, the output δ_z is also reported and the cross-coupling in the (U_y, δ_z)-map is plotted (see Fig. 4-c). The same experiment is also carried out but instead of using $U_z = 0$V, we use non-null and constant values. For instance, in the same figure, we plot the curves obtained with $U_z = 2$V and $U_z = 4$V. Now, we set $U_y = 0$V and we apply a sine input voltage $U_z(t) = 10\sin(2\pi ft)$ with the same frequency $f = 1$Hz. The resulting displacement δ_z versus the voltage, i.e. (U_z, δ_z)-map, is plotted in Fig. 4-d (with solid-circle plot) whilst the cross-coupling in the (U_z, δ_y)-map is plotted in Fig. 4-b. Similarly to the previous

experiment, different non-null and constant values of U_y have also been utlized and the resulting curves are plotted in the same figure. As from these results, the direct transfers (Fig. 4-a and d) are characterized by hysteresis nonlinearities with amplitudes that reach $\frac{h_h}{H_h} = 21\%$. We also observe that the cross-couplings have an amplitude exceeding $-30\mu\text{m} \leftrightarrow 21\mu\text{m} = 51\mu\text{m}$ (see (U_z, δ_y)-map when $U_y = 0\text{V}$). As the maximal displacement reachable in the y-axis when it is actuated (see (U_y, δ_y)-map) is about 50μm, we calculate the relative amplitude of the coupling in the y-axis: $\frac{51\mu m}{50\mu m} = 102\%$. This means that the cross-coupling is stronger than the direct transfer itself. Regarding the z-axis, the relative amplitude of the coupling is of $\frac{37\mu m}{60\mu m} = 62\%$. Finally, we remark that these cross-couplings are also hysteretic. These characterizations show the strong couplings and the strong nonlinearities that typify the 2-DOF piezoactuator.

It is important to notice that the frequency of the signal used to characterize the hysteresis, which is 1Hz in this case, should be chosen sufficiently low in order to avoid the phase-lag caused by the dynamics of the actuator, and not too low in order to avoid the effect of the creep nonlinearity which typifies piezoelectric actuators [43]. Different and extensive characterizations of the piezoactuator used here shown that a good compromise of this characterization frequency is between 0.1Hz and slightly higher than a Hertz. It is also worth to notice that the two sensors employed to measure the displacements along y and z axes should be properly and orthogonally mounted, otherwise the cross-couplings observed will include measurement errors.

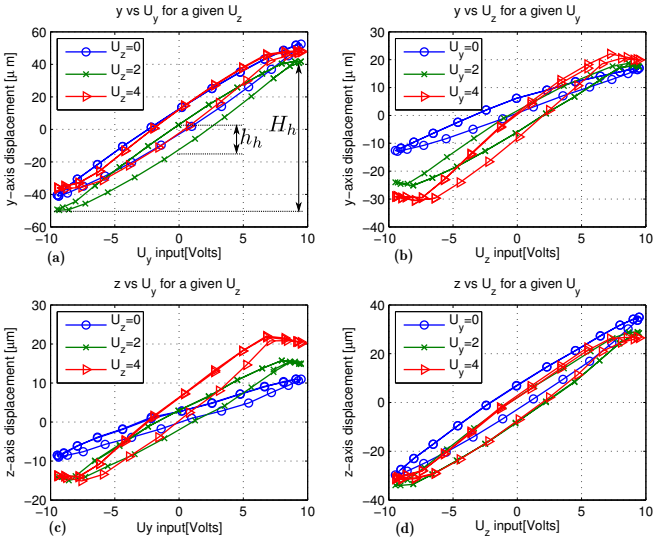

Fig. 4. Hysteresis and cross-couplings characterization.

In order to illustrate the effect of the cross-couplings and of the hysteresis in the precision of the actuator, we have carried out a complex spatial trajectory tracking, by utilizing a linear compensator (a feedforward control with linear gains). The results, when the desired trajectory (reference) is a circle

with 20μm radius and 1Hz frequency, are pictured in Fig. 5-a. The evaluation of the errors in the two axes y and z is described in Fig. 5-b and c respectively. These figures demonstrate that, due to the strong cross-couplings and to the hysteresis nonlinearity, the absolute tracking error (defined as distance between the reference and the output) in the y-axis can reach 12μm whilst that of the z-axis can reach 10.5μm. These errors correspond to relative errors of $60\% = \frac{13\mu m}{20\mu m}$ and $52.5\% = \frac{10.5\mu m}{20\mu m}$ respectively. The spatial curve show that such errors are non-negligible and that the piezoactuator cannot correctly follow the desired trajectory. By increasing the frequency f, the errors increase substantially. It is therefore important to control the piezoactuator with convenient consideration of the cross-couplings and of the hysteresis.

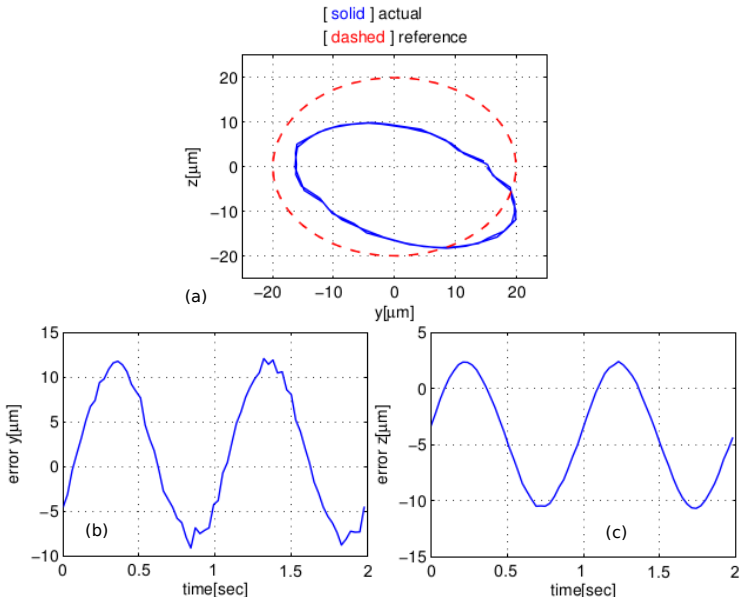

Fig. 5. Open-loop response of the 2-DOF piezoactuator with a circular desired trajectory.

Finally, the dynamics of the piezoelectric actuator is experimentally characterized. The characterization is carried out by using harmonic or frequency analysis. The procedure of the experiments is similar to that of the hysteresis characterization above, but instead of using a sine signal with one frequency, we employ swept sine signal starting from 1Hz (6.28rad/s). Fig. 6-a depicts the frequency response measured at the y-axis. It includes the magnitudes of: i) the direct transfer that links U_y and δ_y (real system), ii) the 2^{nd} order model that approximates this dynamics and that will be further used for the controller design, iii) and the cross-coupling that links U_z and δ_y. The parameters of the identified 2^{nd} order model are: $a_y = 4.136 \times 10^{-8}$ and $b_y = 5.198 \times 10^{-6}$. On the other hand, Fig. 6-b depicts the frequency response measured at the z-axis. It includes the magnitudes of: i) the direct transfer that links U_z and δ_z (real system), ii) the 2^{nd} order model that approximates this dynamics and that will be further used for the controller design, iii) and the cross-coupling that links U_y and δ_z. The parameters of the identified 2^{nd} order model for this

axis are: $a_y = 5.362 \times 10^{-8}$ and $b_y = 4.863 \times 10^{-6}$. These results show that the resonant frequency of the system is of 783Hz (4920rad/s) and of 687Hz (4320rad/s) for the y-axis and for the z-axis respectively, which are very interesting for the targetted tasks. However we observe that the cross-couplings are strong for the two axes: 1.6dB and -1.09dB respectively. As presented in Fig. 5, they greatly compromise the precision of piezoactuator to follow desired trajectory. Furthermore, we can also observe a high Q-factor with a height of 31.9dB and 33.5dB for the y-axis and for the z-axis respectively. These peaks result in badly damped oscillations in the responses of the actuator to brusque inputs (like rectangular) which are unwanted in micromanipulation and in microassembly tasks. The aim of the next section is to propose a control stragety that accounts for the strong cross-couplings and for the nonlinearities in order to reach the performances usually required in the targetted tasks.

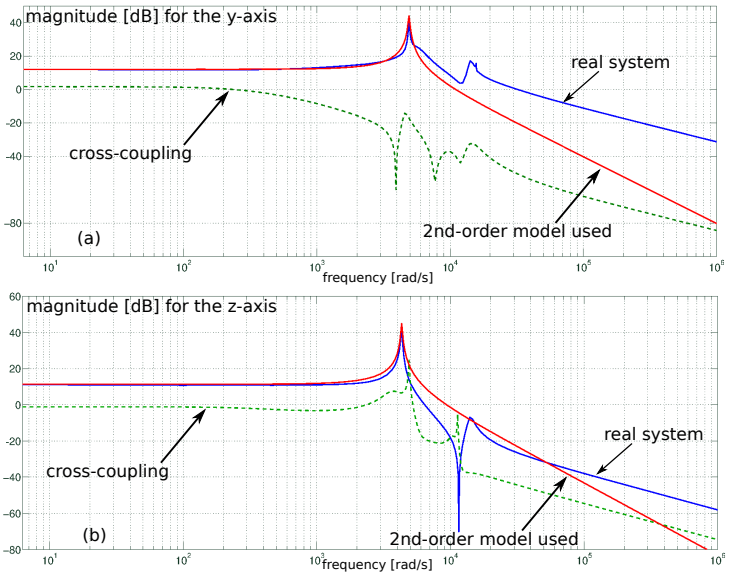

Fig. 6. Open-loop response of the 2-DOF piezoactuator with a circular desired trajectory.

4 Backstepping control of the 2-DOF piezoactuator

In this section, we address the control design for the 2-DOF piezoactuator using the backstepping framework including adaptive and robust actions. The resulting controller is robust enough to deal with model uncertainties, either structured or non-structured, or disturbance provided the knowledge of their bounds. To fulfill the control objective, a sliding surface z, encompassing tracking errors, is defined within the backstepping recursive process so that the states trajectories reach and remain in the origin. On the other hand, the adaptive part, also included in the backstepping design, is used to cope with unknown slow-time varying disturbances [62].

Reconsider the disturbed model of the 2-DOF piezoactuator described in (7):

$$a\ddot{\delta} + b\delta + \delta = d_p U + \Theta \tag{9}$$

Since we are in concern with a trajectory tracking problem, the latter differential model can be rewritten as a state-space model with the error variable $\xi = (\xi_1, \xi_2)^T$:

$$\begin{aligned} \dot{\xi}_1 &= \xi_2 \\ \dot{\xi}_2 &= \tfrac{1}{a}(d_p U + \Theta - b\dot{\delta} - \delta) - \ddot{\delta}^d \end{aligned} \tag{10}$$

where $\xi_1 = \delta - \delta^d$ and $\xi_2 = \dot{\delta} - \dot{\delta}^d$ are the position and the velocity errors respectively.

Step 1: Let us propose the following quadratic Lyapunov function to deduce a control that stabilizes the first integrator subsystem (10-a):

$$\mathcal{V}_1(\xi_1) = \frac{1}{2}\xi_1^T \xi_1 \tag{11}$$

whose time-derivative is given by

$$\dot{\mathcal{V}}_1(\xi) = \xi_1^T \xi_2 \tag{12}$$

which can be rendered negative ($\dot{\mathcal{V}}_1(\xi) < 0$) if we propose ξ_2 as virtual controller defined by the following law:

$$\xi_2 = -\lambda_1 \xi_1 \tag{13}$$

where $\lambda_1 = \text{diag}(\lambda_{1y}, \lambda_{1z})$ with $\lambda_{1y} > 0$ and $\lambda_{1z} > 0$. With this, ξ_1 is not only stable but also asymptotically convergent to the origin.

Step 2: Let us propose the error variable $z = (z_y, z_z)^T$ using the virtual controller as a reference, i.e. $\xi_2^d = -\lambda_1 \xi_1$:

$$z = \xi_2 - \xi_2^d = \xi_2 + \lambda_1 \xi_1 \tag{14}$$

which produces the modified state

$$\xi_2 = z - \lambda_1 \xi_1 \tag{15}$$

Computing the time-derivative of (14) yields:

$$\dot{z} = \frac{1}{a}(d_p U + \Theta - b\dot{\delta} - \delta) + \lambda_1 z - \lambda_1^2 \xi_1 - \ddot{\delta}^d \tag{16}$$

Let us split the overall vector disturbance into two terms: a high- and a low-rate disturbance $\Theta = \Theta_h + \Theta_l$, whose expression is written as:

$$\Theta = \Theta_h + \Theta_l = \begin{pmatrix} \theta_{h_y} + \theta_{l_y} \\ \theta_{h_z} + \theta_{l_z} \end{pmatrix} \tag{17}$$

where Θ_h and Θ_l verifies the following inequalities:

$$\begin{aligned} \|\Theta_h\|_2 &\leq \varepsilon_h \\ \|\Theta_l\|_2 &\leq \varepsilon_l \end{aligned} \tag{18}$$

where ε_h and ε_l are positive scalars. In order to provide the final control Lyapunov function (CLF), let us define the low-rate disturbance estimation error $\tilde{\Theta}_l$ and its derivative as well:

$$\tilde{\Theta}_l = \Theta_l - \hat{\Theta}_l \tag{19}$$

and

$$\dot{\tilde{\Theta}}_l = -\dot{\hat{\Theta}}_l \tag{20}$$

The following final CLF is therefore proposed:

$$\mathcal{V}_2(\xi_1, z) = \frac{1}{2}\xi_1^T \xi_1 + \frac{1}{2} z^T z + \frac{1}{2}\tilde{\Theta}_l^T \gamma^{-1} \tilde{\Theta}_l \tag{21}$$

where $\gamma = \text{diag}(\gamma_y, \gamma_z)$ is a positive definite matrix. The time-derivative of the CLF $\mathcal{V}_2(\xi_1, z)$ is yielded:

$$\dot{\mathcal{V}}_2(\xi_1, z) = -\xi_1^T \lambda_1 \xi_1 + \xi_1^T z + z^T \dot{z} + \tilde{\Theta}_l^T \gamma^{-1} \dot{\hat{\Theta}}_l \tag{22}$$

Replacing $\dot{z}$ of (22) by (16), introducing the following adaptation law

$$\dot{\hat{\Theta}} = -\gamma z \tag{23}$$

and the following proposed controller

$$U = \frac{1}{d_p}[a(-\lambda_1 z + \lambda_1^2 \xi_1 - \xi_1 - \lambda_2 z + \ddot{\delta}^d) + \hat{\Theta}_l + \text{sign}(z) + b\dot{\delta} + \delta] \tag{24}$$

where $\text{sign}(z) = (\text{sign}(z_y), \text{sign}(z_z))^T$, where the gain matrix $\lambda_2 = diag\,(\lambda_{2y}, \lambda_{2z})$ only requires to be positive definite to verify negativity of the time-derivative of the CLF and where $\alpha = diag\,(\alpha_y, \alpha_z)$ is a positive definite matrix;

we obtain:

$$\dot{\mathcal{V}}_2(\xi_1, z) = -\xi_1^T \lambda_1 \xi_1 - z^T \lambda_2 z + z^T(\Theta_h - \alpha \text{sign}(z)) \tag{25}$$

(25) can be simplified as follows:

$$\dot{\mathcal{V}}_2(\xi_1, z) \leq -\rho_{min}\{\lambda_1\}\|\xi_1\|_2^2 - \rho_{min}\{\lambda_2\}\|z\|_2^2 + |z^T\Theta_h| - \alpha\|z\|_1 \tag{26}$$

where $\rho_{min}\{\cdot\}$ stands for the minimun eigenvalue. The latter condition is still satisfied with:

$$\dot{\mathcal{V}}_2(\xi_1, z) \leq -\rho_{min}\{\lambda_1\}\|\xi_1\|_2^2 - \rho_{min}\{\lambda_2\}\|z\|_2^2 + (\varepsilon_h - \alpha)\|z\|_1 \tag{27}$$

where we have used the following properties:

- **P1.** $\|x^T y\|_2 \leq \|x\|_2 \|y\|_2$
- **P2.** $\|x\|_2 \leq \|x\|_1$
- **P3.** $\|x\|_1 = \sum_{i=1}^n |x_i|$
- **P4.** $|x_i| = x^T \text{sign}(x)$

for any vectors x and y with length equal to n.

Therefore, to insure negativity of the time-derivative of the CLF as in (27), we choose:

$$\alpha = \varepsilon_h + \eta \tag{28}$$

which leads to:

$$\dot{\mathcal{V}}_2(\xi_1, z) \leq -\rho_{min}\{\lambda_1\}\|\xi_1\|_2^2 - \rho_{min}\{\lambda_2\}\|z\|_2^2 - \eta\|z\|_1 \tag{29}$$

In order to implement the controller, (14) is introduced in the control law of (24). Then, we take $\lambda_1 = \lambda_2 = \lambda = diag(\lambda_y, \lambda_z)$ which permits to have a simpler expression only dependent on the states of the system. We obtain:

$$\begin{aligned} U = \tfrac{1}{d_p}[a(-(\lambda^2+1)\xi_1 - 2\lambda\xi_2 + \ddot{\delta}^d) \\ + \textstyle\int_0^t \gamma(\xi_2 + \lambda\xi_1)d\tau + \alpha\text{sign}(\xi_2 + \lambda\xi_1) + b\dot{\delta} + \delta] \end{aligned} \tag{30}$$

Fig. 7 shows the implementation diagram of the the whole system where the control law defined by (30) is inside the block "robust adaptive controller". Since the controller requires the derivative of $\delta = (\delta_y, \delta_z)^T$, we utilize an observer to furnish this. The observer, based on the same model than presented in section-2 and developed in our previous work [63], permits to provide an estimate of δ and an estimate of $\dot{\delta}$ in presence of hysteresis nonlinearities. We also tested a direct (numerical) derivative of the measurement δ to provide $\dot{\delta}$. This method is simple in implementation but, in counterpart, introduces an important noise that finally decreases the performances of the whole closed-loop. Notice that the derivative $\dot{\delta}^d$ and the second derivative $\ddot{\delta}^d$ of the desired displacement δ^d are directly yielded by numerical derivative of this latter. The resulting $\dot{\delta}^d$ and $\ddot{\delta}^d$ are not prone to noise since δ^d itself is not from any measurement but generated from Matlab-Simulink.

In the controller (30), the term $\alpha\text{sign}(\xi_2 + \lambda\xi_1)$ is the core of the sliding mode action and the term $\int_0^t \gamma(\xi_2 + \lambda\xi_1)d\tau$ is the core of the adaptive action. It is possible to neglect the two last terms, i.e. $b\dot{\delta} + \delta$, since the controller can compensate for such dynamics with appropriate gains, as will be shown in the experimental section.

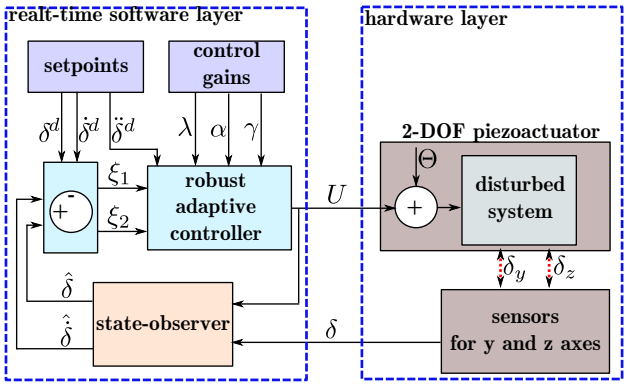

Fig. 7. Overall experimental control setup

To summarize, the controller described above takes into account an overall disturbance (hysteresis + couplings + creep) which is afterwards considered

and handled as an unknown-but-bounded uncertainty. This uncertainty is split into two kinds: fast and slow time varying. The controller is designed via the backstepping approach and the uncertainty has been accounted for during its synthesis in order to guarantee stability. For the fast disturbance we have introduced a sliding-mode term, whereas the slow one is addressed via the adaptive term. Then, the controller performance (robustness) will be guaranteed for the fast-disturbance case provided that its norm remains below the value used within the stability analysis. In the slow-disturbance case the successful estimation will counteract its actual value. The stability robustness of the overall closed-loop system is therefore ensured thanks to the given norms and to estimation performance.

5 Experimental Results

This section is devoted to the experimental tests of the proposed backstepping-based robust adaptive control to the 2-DOF piezoactuator presented in section-3. Whilst tracking of predefined trajectories is the objective, two sets of experiments, both with complex trajectories, were carried out to evaluate the control strategy. In the first set, four waypoints are considered as the reference for different frequency values to obtain a rectangular path. In the second set, circular trajectories are considered to evaluate the tracking performances of the controllers.

5.1 Rectangular waypoints tracking

A periodic square trajectory with sizes 10μm $\times 10\mu$m and at different frequencies is applied in order to evaluate the performance of the proposed control approach. The controller gains used are listed in table 1. he choice of these controller gains will be discussed in section-5.4.

The results with 1Hz of frequency are depicted in Fig 8. In these, the time-domain evolutions (reference tracking and errors) along y and z axes of the piezoactuator are shown in Fig 8-a whilst the spatial trajectory tracking is shown in Fig 8-b. These figures show that the tracking errors, i.e. bias between the output δ_y (resp. δ_z) and the reference δ_y^d (resp. δ_z^d) are negligible, despite the noise mainly due to the sensors used. Indeed, the relative errors in closed-loop are lower than 2% for both axes, whilst in open loop (see section-3) we had 60% and 52.5% for y and z axes respectively. The evaluation of the noise shows a peak-to-peak of $\pm 0.3\mu$m and of $\pm 0.9\mu$m for the y-axis and for the z-axis respectively. It is still possible to reduce this noise by setting a lower bandwidth for the sensors used but this will compromise its capability to

Table 1
Controller gains for the rectangular trajectory.

Frequency (axis-y)	$\lambda_{\mathbf{y}}$	$\gamma_{\mathbf{y}}$	$\alpha_{\mathbf{y}}$
$f = 1$	200	0.5	0
$f = 10$	300	0.5	3
$f = 30$	400	0.5	9
Frequency (axis-z)	λ_z	γ_z	α_z
$f = 1$	160	0.5	0
$f = 10$	500	0.78	0
$f = 30$	400	0.8	2

measure the dynamics of the whole system. It is also possible to use sensors with better performances (optical sensors LC2420 from Keyence). However, implementing two of them to simultaneously measure the two displacements was impossible because of their bulky sizes.

Regarding the cross-couplings, we observe that the effect seen on δ_y (resp. δ_z) due to U_z (resp. U_y) is weak and quickly rejected. In the error curves, the maximal cross-coupling is quantified as $3\% = \frac{0.3\mu m}{10\mu m}$ along δ_y (resp. $6\% = \frac{0.6\mu m}{10\mu m}$ along δ_z) and is afterwards rapidly decreased to zero. As we see, the cross-couplings which were introduced in the disturbance Θ were greatly accounted for by the control law since they were 102% and 62% without the proposed control technique (see section-3). Finally, it is quantified that the settling time of the closed-loop is lower than 25ms which is very convenient for the expected positioning applications.

In order to evaluate the bandwidth of the closed-loop controlled 2-DOF piezoactuator when using square spatial trajectory, we increase the frequency. Fig 9 depict the result for 10Hz and Fig 10 for 30Hz. These results show that the coupling effects remain unchanged, i.e. negligible and quickly rejected, than with 1Hz. In addition to this, the settling time is still less than 25ms for both axes and the errors of tracking remain weak. Beyond 30Hz however, the tracking errors start to slowly increase.

5.2 Circular trajectory tracking

In this part, we utilize circular spatial trajectory as reference, with a radius of 20μm. The corresponding time-domain references are: $\delta_y^d = 20\sin(2\pi f)$ and $\delta_z^d = 20\cos(2\pi f)$. Again, different values of frequency f have been used. The controller gains employed during the experiment here are listed in table 2. The

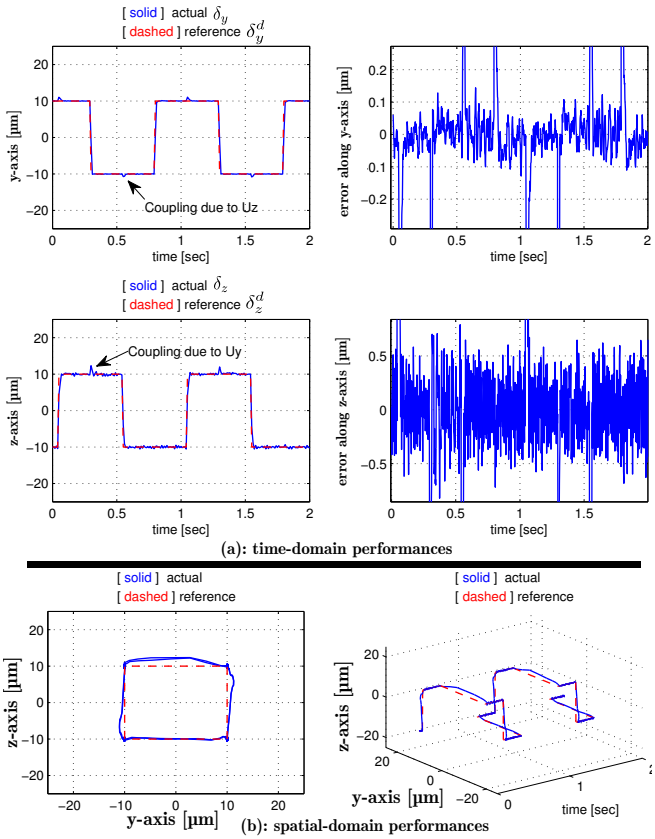

Fig. 8. Closed-loop performances with a square trajectory reference with frequency of 1Hz.

choice of these controller gains will also be discussed in section-5.4.

Table 2
Controller gains for the circular trajectory.

Frequency (axis-y)	$\lambda_{\mathbf{y}}$	$\gamma_{\mathbf{y}}$	$\alpha_{\mathbf{y}}$
$f = 1$	300	1.2	0
$f = 10$	610	1.2	6
$f = 30$	610	1.4	18
Frequency (axis-z)	λ_z	γ_z	α_z
$f = 1$	160	0.8	0
$f = 10$	650	1.4	0.3
$f = 30$	1000	1.2	2

First, a circular reference trajectory with frequency of $1Hz$ was applied. The time-domain results including the reference tracking and the error are pictured in Fig 11-a. We see that the relative error is less than $2.5\% = \frac{0.5\mu m}{20\mu m}$ for the y axis and less than $10\% = \frac{2\mu m}{20\mu m}$ for the z axis, in which the noise can be

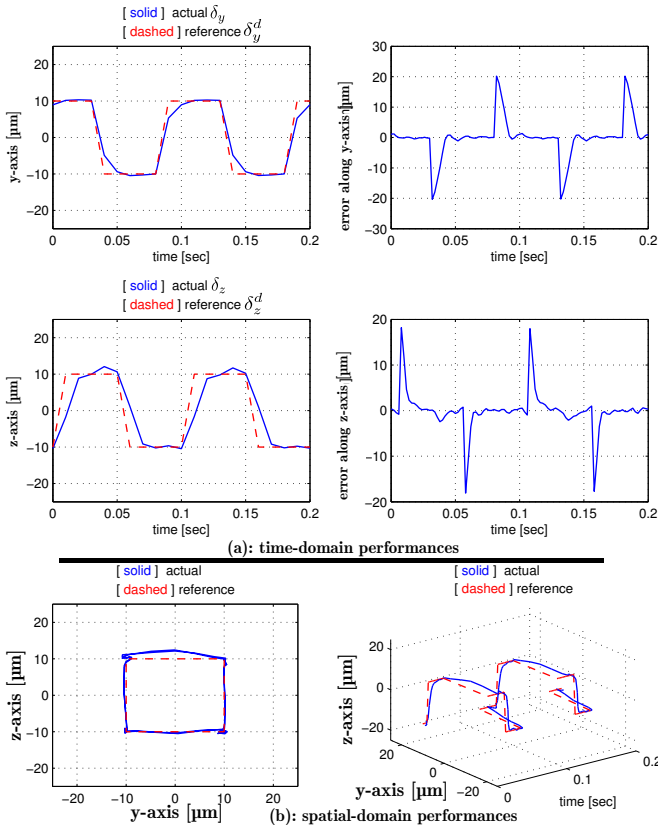

Fig. 9. Closed-loop performances with a square trajectory reference with frequency of 10Hz.

observed as a great part of the error cause. Again, the error was substantially reduced with the proposed control law. In Fig 11-b are pictured the spatial curves which show that the piezoactuator well tracks the circular reference trajectory.

To analyze the capacity of the closed-loop to track higher frequencies for the circular trajectory, we also carried out experiments with 10Hz and 30Hz. The results are depicted in Fig 12 and Fig 13. They show that the tracking error remain almost similar than with low frequency. From 30Hz, this error starts to slowly decrease due to the phase-lag. To analyze the bandwidth and the dynamics of the closed-loop, we present in the next-subsection its frequency responses.

5.3 frequency responses

In this part, we report the frequency responses of the controlled system. The control gains used for the closed-loop are those corresponding to $f = 30$Hz in table 2, i.e. $\lambda_y = 610$, $\gamma_y = 1.4$, $\alpha_y = 18$, $\lambda_z = 1000$, $\gamma_z = 1.2$ and $\alpha_z = 2$. In fact, the control gains tuned at high frequency are also efficient when working

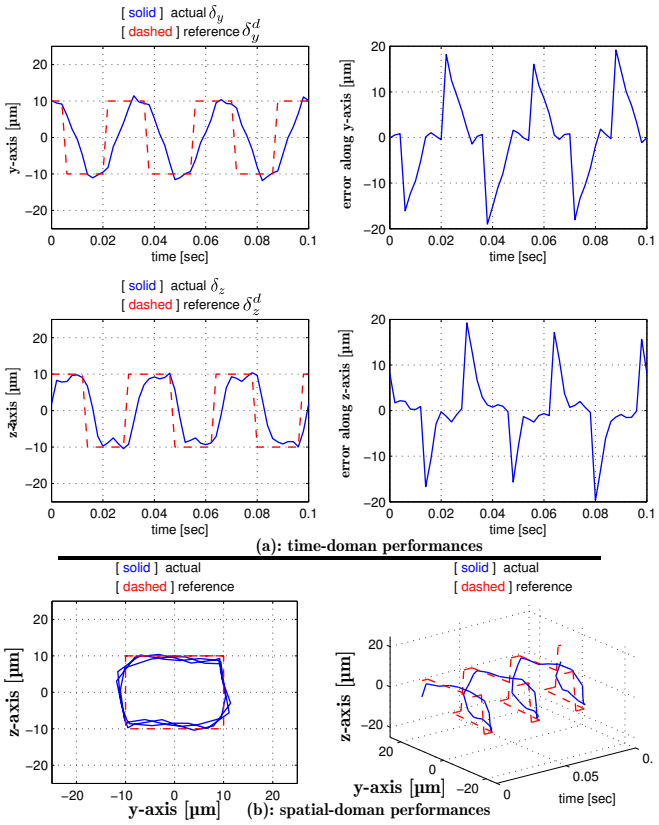

Fig. 10. Closed-loop performances with a square trajectory reference with frequency of 30Hz.

at lower frequencies. Fig 14-a depicts the frequency responses observed at the y-axis: the direct transfer $\frac{\delta_y}{\delta_y^d}$ and the cross-coupling $\frac{\delta_y}{\delta_z^d}$. On the other hand, Fig 14-b depicts the frequency responses observed at the z-axis: the direct transfer $\frac{\delta_z}{\delta_z^d}$ and the cross-coupling $\frac{\delta_z}{\delta_y^d}$. We can observe that the cross-couplings have been reduced thanks to the control law: -40dB and -50dB for the y-axis and for the z-axis respectively. The frequency responses also demonstrate that the $3dB$-bandwidths are of 77Hz (484rad/s) and of 93Hz (589rad/s) for the two axes. These results demonstrate the efficiency of the control law to reject the cross-coupling, to increase the bandwidth and to reduce the initial resonance peaks which were very important (see Fig. 6).

5.4 Discussions

As we can see from table 1 and table 2, different values of the controller parameters $\lambda = diag\,(\lambda_y, \lambda_z)$, $\gamma = diag\,(\gamma_y, \gamma_z)$ and $\alpha = diag\,(\alpha_y, \alpha_z)$ are employed for the different frequencies. The values listed in tables table 1 and table 2 correspond to the chronological tests evolution from low to higher frequency values. However, the gain values calculated at high frequency ($f = 30Hz$ in this case) can be used for every frequency lower than this, either

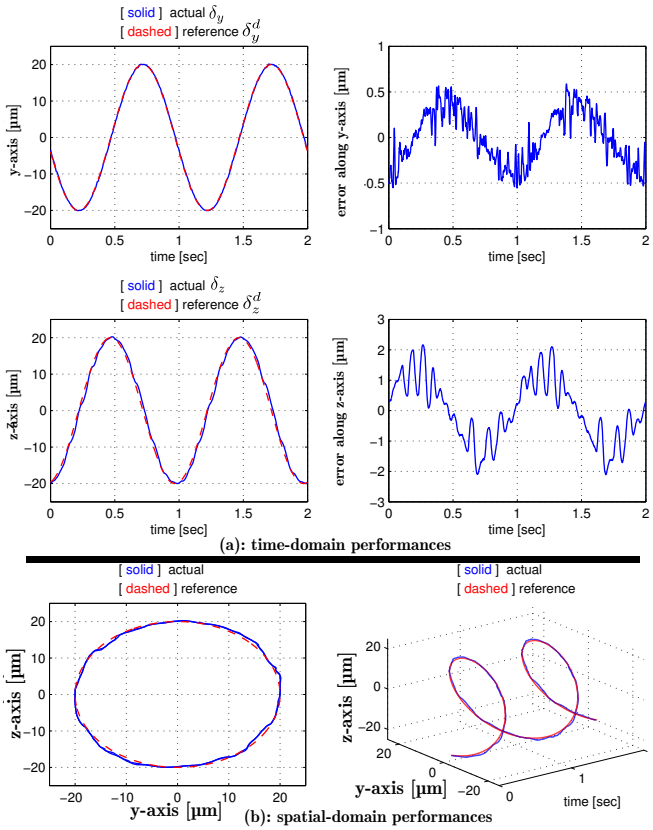

Fig. 11. Closed-loop performances with a circular trajectory reference with frequency of 1Hz.

for rectangular or circular trajectories. If we increase the values of all these parameters, we increase the bandwidth of the closed-loop. A too large value of λ introduces however a low frequency oscillation since this parameter is, among others, used for ξ_2, which is the derivative of ξ_1. Therefore it acts as derivative gain. On the other hand, a too large value of α introduces a high frequency oscillation due to chattering of the sliding mode part. Although, such oscillation will only appear if the gain γ of the adaptive part is very low. Indeed, the adaptive part here is introduced to reduce the chattering of the overall control input. In the experiments carried out, the controller gains were put manually. However, a feature will consist in scheduling them automatically according to the frequency of the input reference δ^d. For that, a way consists in carrying out first a precise performances characterization for different values of controllers gains and at different frequencies. This permits to find the optimal values of the gains for some specified performances. Then, a model of the optimal gains versus the frequencies can be derived. This model can be finally used as a sequencer of the controller.

In this paper, we particularly dealt with second order model of piezoelectric cantilevered actuators. The reason of this is double. First, the control technique requires a second order model only. One of the advantages is that

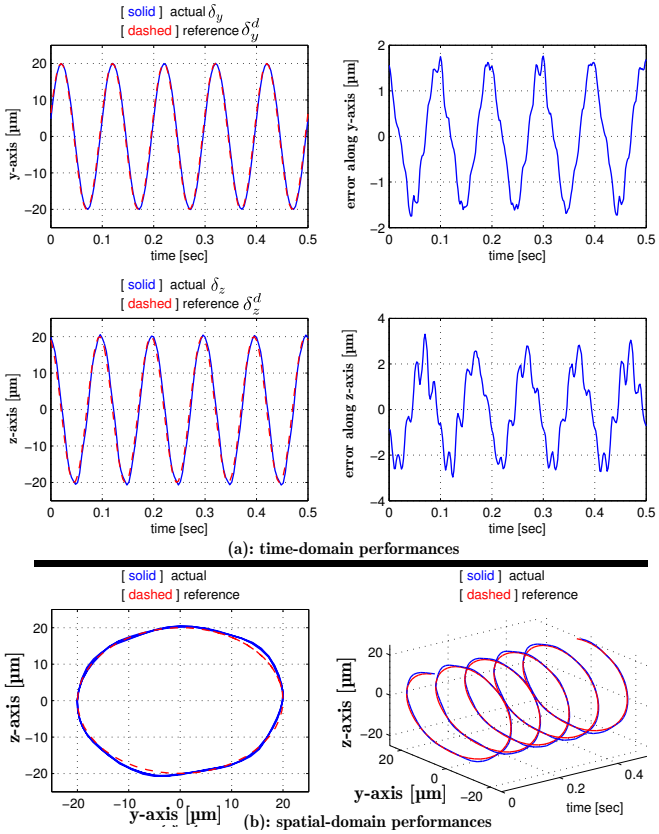

Fig. 12. Closed-loop performances with a circular trajectory reference with frequency of 10Hz.

a simple model is employed to calculate a robust controller. Second, various characterization of the piezoelectric employed in this paper demonstrated that a second order model is largely sufficient to track its dynamics necessary for the targetted applications [10, 57, 61]. Nevertheless, if a higher order model is required, it is still possible to employ the technique as long as the model structure in (10) can be yielded. In such a case, ξ is a vector.

Backstepping technique provides the "right" gains-states combination to guarantee stable states trajectories while rejecting unknown-but-bounded disturbances. "Large" control signals are relative, since our experimental setup features an actuator saturation ranging from -10V to 10V. Therefore, in this case the control signals, provided to the actuator from the dSPACE acquisition board, are bounded and thus the challenge becomes in fulfilling the control objective (trajectory tracking) having bounded control signals. Experimental results proved that the proposed controller was indeed capable to solve the control problem.

The performances observed from the experiments carried out show that the fact of using adaptive and sliding-mode controllers results in a beneficial complementarity reducing bursting errors and chattering. Indeed, it is well known

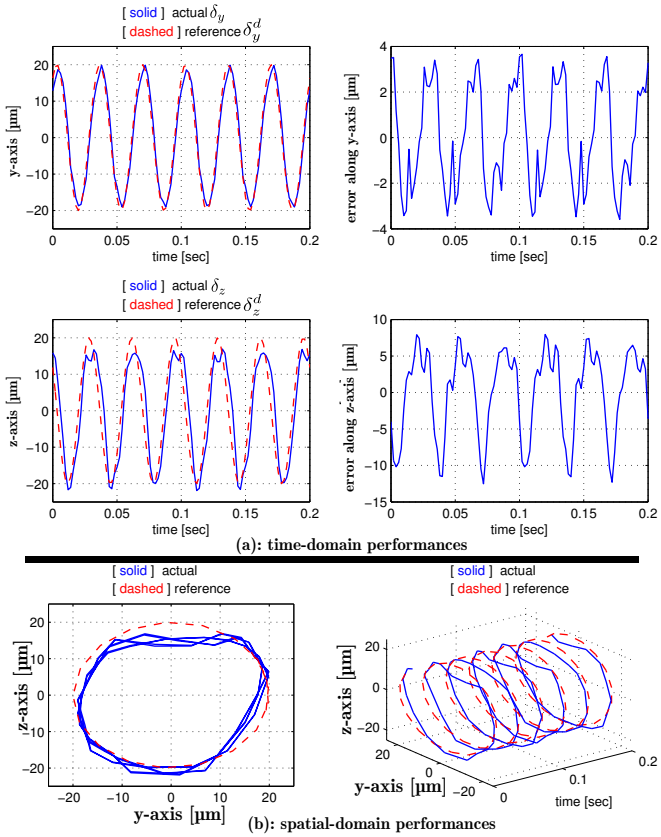

Fig. 13. Closed-loop performances with a circular trajectory reference with frequency of 30Hz.

that bursting errors arise from additive uncertainties (noise, parametric uncertainties) to the adaptive signal and might lead to instability of the closed-loop. In addition, in experimental applications, the chattering associated with the discontinuous control has detrimental effects in the control performance since it may damage the actuator and excite parasitic non-modeled dynamics. These disadvantages have been bypassed in the control law here thanks to the combination of the adaptive and sliding-mode techniques.

Finally, the proposed controller technique has permitted to reduce the cross-couplings to -45dB and -25dB for the y and for the z-axis respectively (see Fig 14), whilst they were about 0dB without control (see Fig. 6). Additionally to this, the initial Q-factors with heights of 31.9dB and 33.5dB for the two axes (see Fig. 6) have been completely reduced. The different experiments with complex trajectories demonstrated that a good tracking precision has been obtained with the closed-loop and the bandwidth were respectively of 77Hz (484rad/s) and of 93Hz (589rad/s) for the two axes. Comparison with classical control design calculated and applied to this same actuator (developed in [57]) demonstrates that the proposed control technique in this paper permits to have better performances simultaneously in term of bandwidth, of cross-couplings rejection and of tracking of complex trajectory. Though well convenient for

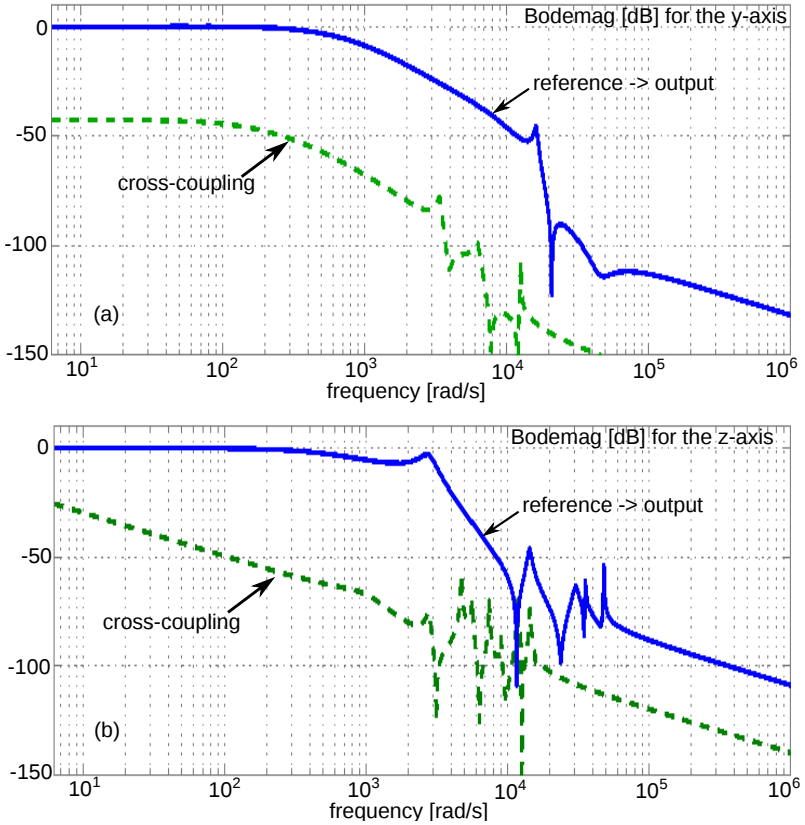

Fig. 14. Frequency responses of the closed-loop.

the tasks targetted in this paper (micromanipulation and microassembly), the bandwidth can be enlarged by finding the controller gains by trial or by an analytical way.

6 Conclusions

The present paper addressed the motion control problem of a piezoelectric actuator while tracking waypoints and smooth (continuous) time-varying trajectories. The actuator has two degrees of freedom (2-DOF) and typifies strong cross-couplings as well as strong hysteresis nonlinearity in its two axes. By extending the classical Bouc-Wen modeling of hysteresis which is devoted to 1-DOF system and by rearranging it, we propose a linear dynamic SISO model with a lumped parameter for each axis. The, parameter, considered as disturbance - which is bounded and which accounts for the hysteresis, for the cross-couplings and for eventual creep nonlinearty - is split into "slow" (quasi-constant) and "fast" (time-varying) parts. Based on the disturbance profile, a backstepping-control strategy merging adaptive (to estimate slow-time varying disturbances) and sliding-mode control (to reject time-varying disturbance) techniques is propposed. The proposed complementary control

scheme provides the following benefits.

- We can estimate the slow-time varying uncertainty/disturbance which regroups hysteresis/cross-couplings (with low frequency inputs) and creep.
- The adaptive part reduces the chattering of the overall control input that may appear due to the sliding-model action.
- The actual approach provides an interesting modularity to tackle constant and/or time-varying disturbances (continous/discontinous).
- The final control law is simple for implementation purposes.

Since the controller gains were introduced manually in this paper, an interesting feature consists in developing a model that relates these gains with the frequency of the input reference for optimal performances. Then, this model can be used as a sequencer for the controller in order to have an automatically gain-scheduled control scheme.

Acknowledgment

This work is supported by the national ANR-Emergence MYMESYS-project (ANR-11-EMMA-006: High Performances Embedded Measurement Systems for multiDegrees of Freedom Microsystems) and partially by the CNRS-project MIM-HAC.

References

[1] G. Binnig and H. Rohrer, "Scanning tunneling microscopy", Helvetica Phys. Acta, vol.55, pp.726-735, 1982.

[2] G. Binnig, C. F. Quate, and C. Gerber, "Atomic force microscope", Phys. Rev. Lett., vol.56(9), pp.930-933, March 1986.

[3] G. Binnig and D. P. E. Smith, "Single-tube three-dimensional scanner for scanning tunneling microscopy", Rev. Sci. Instrum., vol.57(8), pp.1688-1689, Aug. 1986.

[4] R. Merry, M. Uyanik, R. van de Molengraft, R. Koops, M. van Veghel, M. Steinbuch, "Identification, control and hysteresis compensation of a 3 DOF metrological AFM", Asian Journal of Control, vol.11(2), pp.130-143, 2009.

[5] Y.Y. Kuan, K. Liu, and S.O.R. Moheimani, "Reducing cross-coupling in a compliant XY nanopositioner for fast and accurate raster scanning", IEEE Transactions on Control Systems Technology, vo.18(5), pp.1172-1179, 2010.

[6] J. A. Main and E. Garcia, "Piezoelectric stack actuators and control system design: Strategies and pitfalls", J. Guid. Control Dyn., vol.20(3), pp.479-485, May/June 1997.

[7] J. Agnus, P. Nectoux, and N. Chaillet, "Overview of microgrippers and design of a micromanipulation station based on a mmoc microgripper", IEEE International Symposium on Computational Intelligence in Robotics and Automation, pp.117-123, 2005.

[8] M. Rakotondrabe and I.A. Ivan, "Development and Force/Position Control of a New Hybrid Thermo-Piezoelectric microGripper dedicated to micromanipulation tasks", IEEE Transactions on Automation Science and Engineering, Vol.8(4), pp.824-834, 0ctober 2011.

[9] J. Agnus, N. Chaillet, C. Clévy, S. Dembélé, M. Gauthier, Y. Haddab, G. Laurent, P. Lutz, N. Piat, K. Rabenorosoa, M. Rakotondrabe and B. Tamadazte, 'Robotic Microassembly and micromanipulation at FEMTO-ST', Journal of Micro-Bio Robotics (JMBR), Volume 8, Issue 2, Page 91-106, 2013.

[10] M. Rakotondrabe, 'Smart materials-based actuators at the micro/nano-scale: characterization, control and applications', edited book, Springer-Verlag, New York, ISBN 978-1-4614-6683-3, 2013.

[11] S. Devasia, E. Eleftheriou, and S.O.R. Moheimani, "A survey of control issues in nanopositioning", IEEE Transactions on Control Systems Technology, vol.15(5), pp.802-823, 2007.

[12] M. Rakotondrabe, K. Rabenorosoa, J. Agnus, N. Chaillet, "Robust Feedforward-Feedback Control of a Nonlinear and Oscillating 2-DOF Piezocantilever", IEEE Transactions on Automation Science and Engineering, vol.8(3), pp.506-519, July 2011.

[13] M. Rakotondrabe, "Modeling and compensation of multivariable creep in multi-DOF piezoelectric actuators", IEEE International Conference on Robotics and Automation, pp.4577-4581, May 2012.

[14] D. Habineza, M. Rakotondrabe and Y. Le Gorrec, 'Bouc-Wen Modeling and Feedforward Control of multivariable Hysteresis in Piezoelectric Systems: Application to a 3-DoF Piezotube scanner', IEEE Transactions on Control Systems Technology, accepted, to be published in 2015.

[15] E. Zergeroglu et al., "Adaptive set-point control of robotic manipulators with amplitude-limited control inputs", Robotica, vol.18, pp.171-181, 2000.

[16] J. J. Bongiorno Jr, "On the response of linear systems to inputs with limited amplitudes and slopes", SIAM Review, vol. 9(3), pp.554-563, 1967.

[17] G. S. Choi, H-S Kim and G. H. Choi, "A study on position control of piezoelectric actuators", IEEE International Symposium on Industrial Electronics, pp.851-855, July 1997.

[18] B. J. Kenton and K.K. Leang, "Design and Control of a Three-Axis Serial Kinematic High-Bandwidth Nanopositioner", IEEE/ASME Transactions on Mechatronics, vol.17(2), pp.356-369, April 2012.

[19] I. Soltani Bozchalooi, K. Youcef-Toumi, "Multi-actuation and PI control: A simple recipe for high-speed and large-range atomic force microscopy", Ultramicroscopy, Volume 146, pp.117-124, 2014.

[20] M. Rakotondrabe, Y. Haddab and P. Lutz, 'Plurilinear modeling and discrete μ-synthesis control of a hysteretic and creeped unimorph piezoelectric cantilever', IEEE International Conference on Automation, Robotics, Control and Vision, pp:57-64, Grand Hyatt Singapour, Dec 2006.

[21] A. Sebastian, M. V. Salapaka, and J. P. Cleveland, "Robust control approach to atomic force microscopy", Conference on Decision and Control, (Maui, HI), pp. 3443-3444, Dec. 2003.

[22] S. Salapaka, A. Sebastian, J.P. Cleveland and M. Salapaka, "High bandwidth nano-positioner : A robust control approach", Review of scientific instruments, vol.73, pp.3232-3241, 2002.

[23] N. Chuang and I.R. Petersen, "Robust H Infinity Control of Hysteresis in a Piezoelectric Stack Actuator", IFAC World Congress, Vol.17(1), 2008.

[24] I. A-T. Mahmood, K. Liu, S.O.R. Moheimani, "Two Sensor Based H-Infinity Control of a Piezoelectric Tube Scanner", IFAC World Congress, Seoul Korea, July 2008.

[25] G. Schitter, P. Menold, H.F. Knapp, F. Allgöwer, A. Stemmer, "High performance feedback for fast scanning atomic force microscopes", Review of Scientific Instruments, vol.72(8), 2001.

[26] A.J. Fleming, S.S. Aphale and S.O.R. Moheimani, "A new method for robust damping and tracking control of scanning probe microscope positioning stages", IEEE Transactions on Nanotechnology, vol.9(4), pp.438-448, 2010.

[27] Q. Xu and Y. Li, "Global sliding mode-based tracking control of a piezo-driven xy micropositioning stage with unmodeled hysteresis", IEEE/RSJ International Conference on Intelligent Robots and Systems, pp.755-760, October 2009.

[28] S. Yu, B. Shirinzadeh, G. A. and J. Smith, "Sliding mode control of a piezoelectric actuator with neural network compensating rate-dependent hysteresis", IEEE International Conference on Robotics and Automation, pp.3641-3645, April 2005.

[29] X. Chen and T. Hisayama, "Adaptive sliding-mode position control for piezo-actuated stage", IEEE Transactions on Industrial Electronics, vol.55(11), pp.3927-3934, 2008.

[30] H.C. Liaw, B. Shirinzadeh and J. Smith, "Enhanced sliding mode motion tracking control of piezoelectric actuators", Sensors and Actuators A: Physical, vol.138(1), pp.194-202, 2007.

[31] M.S. Sofla, S. M. Rezaei, M. Zareinejad and M. Saadat, "Hysteresis-observer based robust tracking control of piezoelectric actuators", American Control Conference, pp.4187-4192, June 2010.

[32] S. Tien, Q. Zou, and S. Devasia, "Iterative control of dynamics- coupling-caused errors in piezoscanners during high-speed AFM operations," IEEE T. Contr. Syst. T. , vol. 13, no. 6, 2005

[33] U. Aridogan, Y. Shan, K.K. Leang, "Design and analysis of discrete-time repetitive control for scanning probe microscopes"" ASME Journal of dynamic systems, measurement, and control, vol.131(6), 2009.

[34] N. Tamer, M. Dahleh, "Feedback control of piezoelectric tube scanners", Conference on Decision and Control, pp.1826-1831, Lake Buena Vista, FL USA 1994.

[35] S Kuiper, G Schitter, "Model-based feedback controller design for dual actuated atomic force microscopy", IFAC Mechatronics, vol.22(3), 2012.

[36] D. Hughes and J. T. Wen, "Preisach modeling of piezoceramic and shape memory alloy hysteresis", Smart Materials and Structures, Vol.4, pp.287-399, 1997.

[37] D. Croft, G. Shed and S. Devasia, "Creep, hysteresis and vibration compensation for piezoactuators: atomic force microscopy application", ASME Journal of Dynamic Systems, Measurement and Control, vol.123(1), pp.35-43, nov. 1999.

[38] A. Dubra, J. Massa and C.L. Paterson, "Preisach classical and nonlinear modeling of hysteresis in piezoceramic deformable mirrors", Optics Express, Vol.13(22), pp.9062-9070, 2005.

[39] R.V. Iyer, X. Tan and P.S. Krishnaprasad, "Approximate inversion of the Preisach hysteresis operator with application to control of smart actuators", IEEE Transactions on Automatic Control, vol.50(6), pp.798-810, June 2005.

[40] K. Kuhnen and H. Janocha, "Inverse feedforwrad controller for complex hysteretic nonlinearities in smart-materials systems", Control of Intelligent System, Vol.29(3), 2001.

[41] W.T. Ang, P.K. Kholsa and C.N. Riviere, "Feedforward controller with inverse rate-dependent model for piezoelectric actuators in trajectory-tracking applications", IEEE/ASME Transactions on Mechatronics, Vol.12(2), pp.134-142, April 2007.

[42] B. Mokaberi and A. A. G. Requicha, "Compensation of scanner creep and hysteresis for AFM nanomanipulation", IEEE Transactions on Automation Science and Engineering, Vol.5(2), pp.197-208, 2008.

[43] M. Rakotondrabe, C. Clevy and P. Lutz, "Complete open loop control of hysteretic, creeped, and oscillating piezoelectric cantilevers", IEEE Transactions on Automation Science and Engineering, vol.7(3), pp.440-450, 2010.

[44] M. Rakotondrabe, "Classical Prandtl-Ishlinskii modeling and inverse multiplicative structure to compensate hysteresis in piezoactuators", American Control Conference, pp.1646-1651, Montréal Canada, June 2012.

[45] M. Al Janaideh, P. Krejci, "Inverse Rate-Dependent Prandtl-Ishlinskii Model for Feedforward Compensation of Hysteresis in a Piezomicropositioning Actuator", IEEE/ASME Transactions on Mechatronics, vol.18(5), pp.1498-1507, Oct. 2013.

[46] R. Bouc, "Forced vibration of mechanical systems with hysteresis", Conference on Nonlinear Oscillation, Prague, 1967.

[47] Y. K. Wen, "Method for random vibration of hysteresis systems", Journal of the Engineering Mechanics Division, Vol.102(2), pp.249-263, March/April 1976.

[48] M. Rakotondrabe, "Bouc-Wen modeling and inverse multiplicative structure to compensate hysteresis nonlinearity in piezoelectric actuators", IEEE Transactions on Automation Science and Engineering, vol.8(2), pp.428-431, april 2011.

[49] L.E. Malvern, "Introduction to the Mechanics of a Continuous Medium", chapter 6, Prentice-Hall, Englewood Cliffs, NJ, USA, pp.313-319, 1969.

[50] Q. Yang and S. Jagannathan, "Creep and hysteresis compensation for nanomanipulation using atomic force microscope", Asian Journal of Control, vol.11(2), pp.182-187, 2009.

[51] D. Croft, G. Shedd and S. Devasia, "Creep, hysteresis, and vibration compensation for piezoactuators: atomic force microscopy application", American Control Conference, vol.3, pp.2123-2128, 2000.

[52] H. Jung, Y.S. Jong and G. DaeGab, "New open-loop actuating method of piezoelectric actuators for removing hysteresis and creep", Review of Scientific Instruments, vol.71(9), pp.3436-3440, 2000.

[53] R. Changhai and L. Sun, "Hysteresis and creep compensation for piezoelectric actuator in open-loop operation", Sensors and Actuators A: Physical, vol.122(1), pp.124-130, 2005.

[54] P. Ge and M. Jouaneh, "Tracking control of a piezoceramic actuator", IEEE Transactions on Control Systems Technology, vol.4(3), pp.209-216, 1996.

[55] R. Changhai and L. Sun, "Improving positioning accuracy of piezoelectric actuators by feedforward hysteresis compensation based on a new mathematical model", Review of Scientific Instruments, vol.76(9), 2005.

[56] G.M. Clayton, S. Tien, K.K. Leang, Q. Zou and S. Devasia, "A review of feedforward control approaches in nanopositioning for high-speed SPM", ASME Journal of Dynamic Systems, Measurement and Control, vol.131(6), 2009).

[57] M. Rakotondrabe, J. Agnus and P. Lutz, "Feedforward and IMC-feedback control of a nonlinear 2-DOF piezoactuator dedicated to automated micropositioning tasks", IEEE International Conference on Automation Science and Engineering, pp.393-398, Trieste Italy, August 2011.

[58] L. Y. Pao, J. A. Butterworth, and D. Y. Abramovitch, "Combined feedforward/feedback control of atomic force microscopes," in Proc.Amer. Ctrl. Conf., (New York, NY), July 2007.

[59] K.K. Leang and S. Devasia, Senior Member"Feedback-Linearized Inverse Feedforward for Creep, Hysteresis, and Vibration Compensation in AFM Piezoactuators", IEEE Trans. Control Systems Technology, vol.15(5), 2007.

[60] T. S. Low and W. Guo, "Modeling of a three-layer piezoelectric bimorph beam with hysteresis", Journal Microelectromechanical Systems, Vo.4(4), pp.230-237, December 1995.

[61] J. A. Escareno, D. Habineza and M. Rakotondrabe, "Tracking Control of a Piezocantilever Using a Bounded-Input Adaptive Backstepping Scheme and Sliding-Mode Observer", IFAC World Congress, Cape Town, South Africa, August 2014.

[62] J.-J.E. Slotine and W. Li, "Applied nonlinear control", Prentice Hall, ISBN-10:0130408905, 1991.

[63] M. Rakotondrabe and P. Lutz, 'Force estimation in a piezoelectric cantilever using the inverse-dynamics-based UIO technique', IEEE International Conference on Robotics and Automation, pp:2205-2210, Kobe Japan, May 2009.